

SinGeo: Unlock Single Model’s Potential for Robust Cross-View Geo-Localization

Yang Chen¹, Xieyuanli Chen^{1*}, Junxiang Li¹, Jie Tang¹, Tao Wu^{1*}
¹National University of Defense Technology

Abstract

Robust cross-view geo-localization (CVGL) remains challenging despite the surge in recent progress. Existing methods still rely on field-of-view (FoV)-specific training paradigms, where models are optimized under a fixed FoV but collapse when tested on unseen FoVs and unknown orientations. This limitation necessitates deploying multiple models to cover diverse variations. Although studies have explored dynamic FoV training by simply randomizing FoVs, they failed to achieve robustness across diverse conditions—implicitly assuming all FoVs are equally difficult. To address this gap, we present SinGeo, a simple yet powerful framework that enables a **Single** model to realize robust cross-view **Geo**-localization without additional modules or explicit transformations. SinGeo employs a dual discriminative learning architecture that enhances intra-view discriminability within both ground and satellite branches, and is the first to introduce a curriculum learning strategy to achieve robust CVGL. Extensive evaluations on four benchmark datasets reveal that SinGeo sets state-of-the-art (SOTA) results under diverse conditions, and notably outperforms methods specifically trained for extreme FoVs. Beyond superior performance, SinGeo also exhibits cross-architecture transferability. Furthermore, we propose a consistency evaluation method to quantitatively assess model stability under varying views, providing an explainable perspective for understanding and advancing robustness in future CVGL research. Codes are available at: <https://github.com/Yangchen-nudt/SinGeo>.

1. Introduction

Cross-view geo-localization (CVGL) is a geographic location technology by cross-view matching ground-view query image with Geo-tagged satellite database images [6, 9]. This task holds broad application potential in robotic navigation [7], autonomous driving and augmented reality [26].

Traditional CVGL approaches [3, 30, 33] have mainly focused on idealized benchmarks [10, 29] where ground-view images are north-aligned panoramas, and performance on

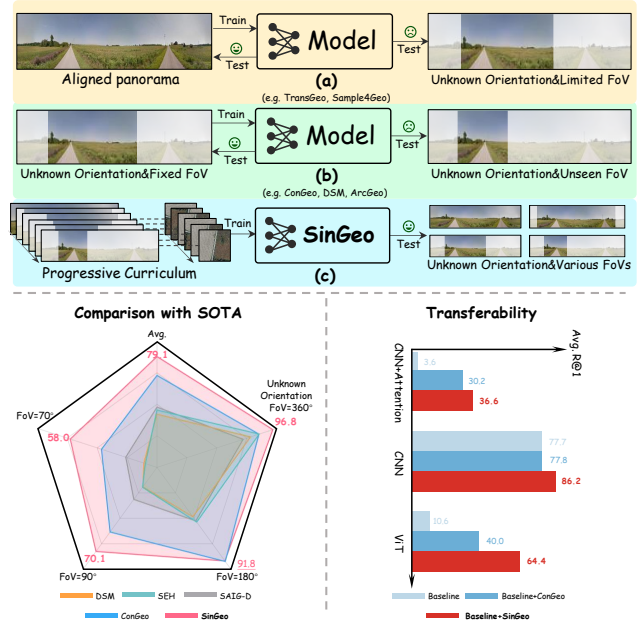


Figure 1. Comparison of different training paradigms for Cross-view Geo-localization. SinGeo achieves superior overall performance and better transferability under scenarios of both unknown orientation and different limited field of views. Previous methods including DSM [20], SEH [5], SAIG-D [34], and ConGeo [13] are reported with their Top-1 Recall performance on CVUSA [29] dataset.

these datasets has largely saturated. However, this paradigm limits the practical utility of CVGL [3] as shown in Fig. 1(a). In real-world practice, ground images are typically captured by consumer-grade devices such as smartphones or vehicle cameras [13]. These images have unknown orientations and restricted FoV, often ranging from 70° to 180°. Such discrepancies introduce significant domain gaps, making robustness and generalization crucial for the wide adoption of CVGL in practical scenarios.

Although recent studies [13, 16, 20] have made progress in robust CVGL, existing methods still face key limitations. Some rely on explicit view transformations, such as polar transformation [20, 23] or bird’s-eye-view projections to reduce the cross-view discrepancy [22]. While simplifying the

*Corresponding authors.

task via unified perspective learning, these designs inevitably introduce image distortions and depend on predefined parameters [22]. More recent robust CVGL methods [16, 23, 26] tackle the problem from the perspective of data augmentation, generating fixed-FoV samples from panoramas [13] and refining architectures or training strategies. However, such a FoV-specific training paradigm leads to good performance only at the trained FoV, and degrades drastically on unseen FoVs as shown in Fig. 1(b). In this context, different models are required for different configurations. These observations raise an important research question: *without explicit transformations or additional modules, can a single model inherently achieve consistent and high performance under varying orientations and FoVs?*

To answer it, we propose SinGeo, a simple yet effective and transferable framework that enhances a single model’s robustness across diverse viewing conditions. SinGeo integrates two synergistic ideas: 1) a dual discriminative learning architecture that strengthens intra-view discriminability for each branch; 2) a progressive training strategy inspired by curriculum learning [2] as shown in Fig. 1(c), that schedules learning difficulty to guide the model from simple to more challenging scenarios. SinGeo consistently achieves strong and balanced performance across varying FoVs and orientations, surpassing previous FoV-specific approaches even under extreme FoV conditions.

To further investigate the mechanism behind improved robustness, we quantitatively measure how consistent a model remains under orientation and FoV variations. This evaluation provides a perspective for understanding and advancing robustness in future CVGL research. We summarize our contributions as follows:

- We present SinGeo, to our best knowledge, the first framework to introduce curriculum learning into robust CVGL. It achieves SOTA performance in robust CVGL across four benchmark datasets. Notably, SinGeo significantly outperforms FoV-specific methods under extreme FoVs.
- SinGeo can be integrated into multiple CVGL backbones, including ViT [4], CNN [11], and CNN+attention [30], consistently enhancing their robustness and outperforming another plug-and-play method, ConGeo [13].
- We provide a new evaluation perspective. Through quantitative consistency analysis, we provide valuable insights into the robustness and stability of CVGL models, offering a potential direction for future research to measure robustness in CVGL.

2. Related work

Traditional Cross-View Geo-Localization. In CVGL studies, a common paradigm to perform cross-view matching [6, 21] is extracting feature embeddings independently from ground-view and satellite images, and then aligning their similarities through various contrastive learning loss functions

[3, 5, 23, 24, 29]. Early approaches attempted to explicitly bridge the cross-view gap. Shi *et al.* [19, 20] converted satellite images into pseudo ground-view representations via polar transformation. Alternatively, some methods [22, 28] projected ground-view imagery or intermediate features into bird’s-eye view. Yet, such transformation-based pipelines tend to introduce distortions that degrade features [3].

More recent research has shifted toward transformation-free architectures that align representations through advanced network design. TransGeo [33] proposed the first pure transformer-based method achieving better performance. Besides, hybrid CNN–Attention frameworks [19, 30] leveraging local–global feature extraction further improved representation ability. Notably, Sample4Geo [3] used a single CNN encoder with InfoNCE loss [14] and proposed new hard negative sampling strategies, reaching competitive performance without additional modules or transformations.

As also discussed in [3], benchmarks such as CVUSA [29] and CVACT [10] with north-aligned and center-aligned panoramas are becoming saturated. Previous methods collapse severely under practical conditions where images have unknown orientation and narrow FoV [13].

Robust Cross-View Geo-Localization. Robust CVGL focuses on maintaining performance under unknown orientation and limited FoV conditions. Shi *et al.* [20] pioneered this line of work with the DSM module, which uses a fixed sliding window over the query-activated region for orientation estimation and robust matching. Follow-up studies mainly explored strategies based on data augmentation. For scenarios with unknown orientation, DeHi [26] contrasted representations of polar-transformed satellite images and unaligned panoramas. For scenarios with both unknown orientation and limited FoVs, models such as GAL [16] and ArcGeo [23] randomly shifted and cropped panoramas into fixed FoV patches, substituting them for the original panoramic inputs to strengthen their limited-FoV representations. Specifically, ConGeo [13] provided a novel approach to align embeddings from panoramas and their cropped ones under particular FoVs, thus enhancing its performance in the corresponding limited-FoV occasions.

However, existing studies focus more on the ground branch, overlooking the satellite one. More noteworthy, most of them train their models solely at one particular FoV. While effective at the trained FoV, these models collapse when tested at unseen ones. Developing a method or even a paradigm that performs uniformly across limited FoVs remains a crucial and unsettled endeavor.

Curriculum Learning. Curriculum Learning (CL) [2], first proposed by Bengio *et al.* with convergence proof, was inspired by the human learning progress from easy to difficult tasks. Li *et al.* [8] apply CL to the unsupervised learning paradigm in traditional CVGL. Yet, CL remains underexplored in robust CVGL. Few studies explore the potential

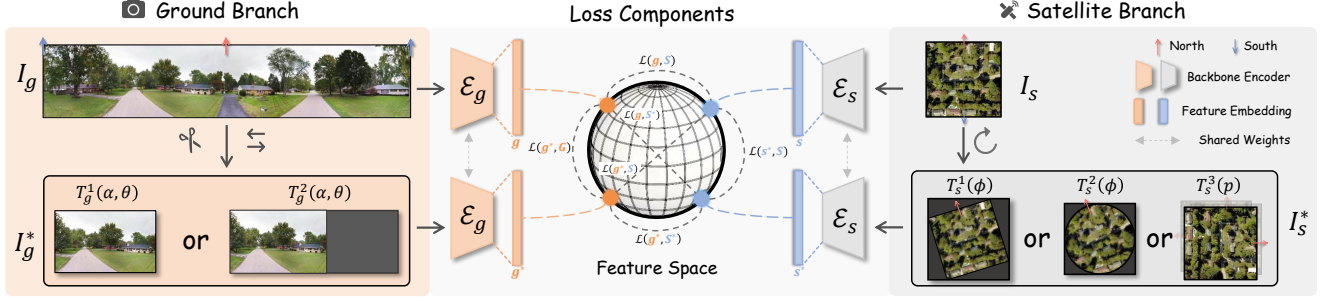


Figure 2. The proposed dual discriminative learning architecture. “Dual” denotes the two-branch design that enhances intra-view discriminativeness through self-supervision in both ground and satellite branches. Specifically, each branch applies specific transformations to generate I_g^* and I_s^* . The learning objective combines contrastive losses for intra-view discrimination and cross-view alignment.

of training with dynamic FoVs. ConGeo [13] and TransGeo [33] tried training models with 0° – 360° random FoVs, but underperformed their fixed-FoV setups. This design implicitly assumes all FoVs are equally difficult. Our work aims to question this assumption by introducing a CL-inspired strategy that enables a single model to perform effectively and consistently at different FoVs.

3. SinGeo

To unleash a single model’s potential for robust CVGL, we propose SinGeo, a dual discriminative learning architecture coupled with a curriculum learning strategy. Notably, both of them are module-free, granting SinGeo model-agnostic properties and allowing integration with different CVGL backbones.

3.1. Dual Discriminative Learning

Traditional CVGL methods mainly align cross-view features via contrastive losses [14, 17, 24], but objectives like InfoNCE [14] can lead to shortcut solutions [15]. Although prior work [13, 16] improves single-branch representations, a unified design equally enhancing both branches remains underexplored. Under limited FoV and unknown orientation, strong intra-view discriminability is crucial for extracting meaningful features.

Contrastive Learning for Discriminativeness. We denote the ground-view image as I_g and the satellite image as I_s , with their corresponding encoders \mathcal{E}_g and \mathcal{E}_s .

To enhance the discriminativeness of the model, we first generate positive samples I_g^* with unknown orientation and limited FoV, following previous studies [13, 23]. This approach aims to create new positive sample pairs (I_g, I_g^*) , reducing the feature distance between I_g and I_g^* so that they can be aligned with I_s in a more unified feature space.

In fact, we observe that another feasible way to create sample pairs under unaligned orientation is to rotate the satellite image I_s to I_s^* , thereby generating another set of positive sample pairs (I_s, I_s^*) . This design essentially enables the

model to focus on discriminative regions in I_s through self-supervision, rather than merely learning the correspondence between I_s and I_g .

This dual design as shown in Figure 2 allows the model to focus on both the satellite branch and the ground branch themselves, and prevents the model from “bias” such as over-focusing on a single branch, or blindly searching for corresponding parts between satellite images and ground view images during training while forgetting to extract features of truly important regions in each branch.

Specifically, the loss for discriminativeness is given by

$$\mathcal{L}(g^*, G) = -\log \frac{\exp(g^* \cdot g_+/\tau)}{\sum_{g_i \in G} \exp(g^* \cdot g_i/\tau)}, \quad (1a)$$

$$\mathcal{L}(s^*, S) = -\log \frac{\exp(s^* \cdot s_+/\tau)}{\sum_{s_i \in S} \exp(s^* \cdot s_i/\tau)}, \quad (1b)$$

$$\mathcal{L}_{\text{disc}} = \mathcal{L}(g^*, G) + \mathcal{L}(s^*, S). \quad (2)$$

g and g^* denote the encoded embeddings of I_g and I_g^* , respectively. G represents the set of embeddings encoded from a collection of $\{I_g\}$, where $g_+ \in G$ is the only positive sample matching g^* , and the rest of G are all negative samples. s, s^*, s_+ , and S are defined analogously.

As illustrated in Fig. 2, we utilize several transformation alternatives to generate I_g^* and I_s^* . For the ground-view branch, two distinct transformations $T_g^1(\alpha, \theta)$ and $T_g^2(\alpha, \theta)$ are applied. For CNN-based models, T_g^1 randomly shifts the panorama horizontally by an angle α and crops a view with FoV θ . For ViT-based models, T_g^2 further pads the cropped view with zeros into the original panorama size. For the satellite branch, we consider two continuous rotation transformations, $T_s^1(\phi)$ and $T_s^2(\phi)$, and a discrete one $T_s^3(p)$. Here, ϕ denotes the angle of yaw rotation. $T_s^1(\phi)$ and $T_s^2(\phi)$ perform outer- and inner-bounding rotations, respectively. $T_s^3(p)$ applies a clockwise rotation by one of $\{90^\circ, 180^\circ, 270^\circ\}$ with probability p . All transformations additionally include color-level augmentations, such as variations in brightness and saturation.

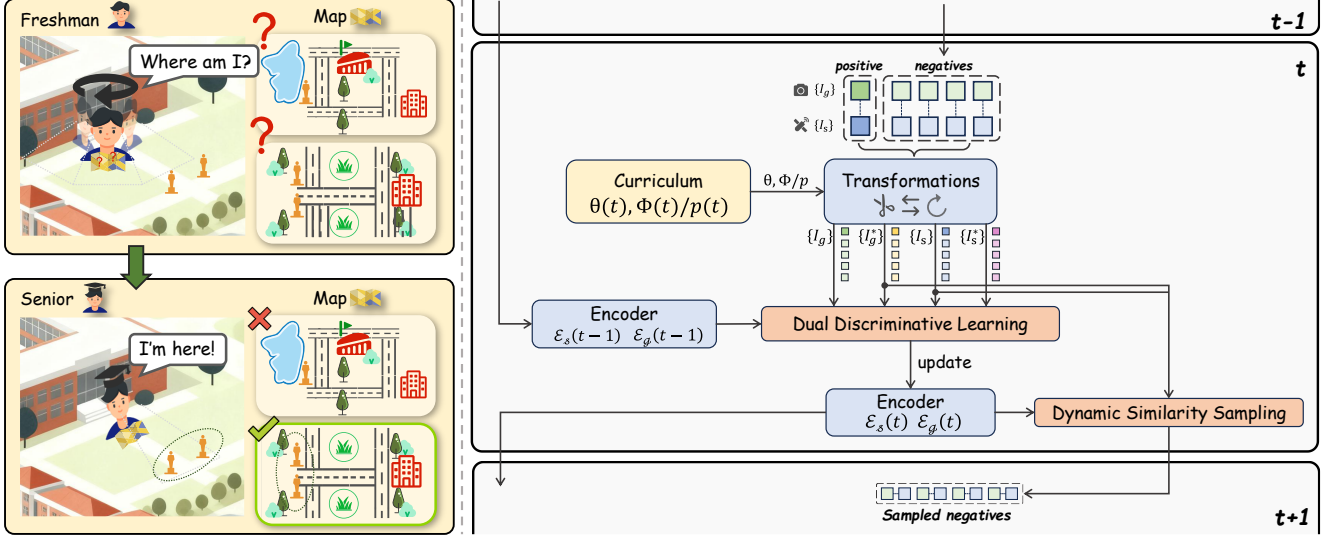


Figure 3. Illustration of the curriculum learning framework and its inspiration. Left: An intuitive analogy of curriculum learning, where a freshman gradually refines geo-localization ability when he gets more familiar and practiced. Right: The predetermined curriculum schedules the difficulties according to the epoch t . After updated by dual discriminative learning, the encoder is then fed into Dynamic Similarity Sampling block [3] to generate negatives for next epoch.

Contrastive Learning for Cross-view Alignment. After collecting a richer set of cross-view samples (I_g, I_s, I_g^*, I_s^*) , we introduce the cross-view learning loss of SinGeo to perform feature alignment between different views, defined as

$$\mathcal{L}_{\text{cross}} = \mathcal{L}(g, S) + \omega_1 \mathcal{L}(g^*, S) + \omega_2 \mathcal{L}(g, S^*) + \omega_3 \mathcal{L}(g^*, S^*), \quad (3)$$

where each loss term $\mathcal{L}(\cdot, \cdot)$ follows the similar definition in Eq. (1a)–(1b), and $\omega_1, \omega_2, \omega_3$ are balancing weights of the augmented sample pairs. Finally, the training objective of SinGeo is

$$\mathcal{L}_{\text{total}} = \mathcal{L}_{\text{cross}} + \gamma \mathcal{L}_{\text{disc}}, \quad (4)$$

where γ is a trade-off factor that balances discriminativeness and cross-view alignment.

3.2. Curriculum Learning for Robust CVGL

In Fig. 3, we recall how human learn cross-view geo-localization in everyday experience. When inexperienced or unfamiliar with a location, individuals initially conduct a 360° panoramic scan and then match the visual context with a map to infer their position. With increased familiarity or experience, they can pinpoint their location on the map via a limited FoV instead of panoramic observation.

Inspired by this observation and curriculum learning, we enable the CVGL model to learn progressively. As illustrated in Fig. 3, the proposed curriculum learning (CL) process dynamically modulates the generation of (I_g, I_s, I_g^*, I_s^*) during training according to the current epoch t . After each update via backpropagation of the dual discriminative learning loss,

the updated encoders $\mathcal{E}_g(t)$ and $\mathcal{E}_s(t)$ perform Dynamic Similarity Sampling [3] on I_g^* and I_s to mine new sampled negatives for the next epoch based on visual similarity.

To realize this progressive training process, we dynamically adjust $T_g(\alpha, \theta)$ and $T_s(\phi)$ or $T_s(p)$ to enable an easy-to-hard transition over epochs. Specifically, let the total training epochs be n , and the current epoch be t . To achieve this, we parameterize the dynamic evolution of the parameters θ, ϕ , and p as functions of the training progress t/n .

Formally, let $\eta \in \{\theta, \phi, p\}$ denote a generic parameter, with initial value η_{init} and final value η_{final} corresponding to an easy beginning and a hard ending respectively.

$$\eta(t) = \eta_{\text{init}} + (\eta_{\text{final}} - \eta_{\text{init}}) \cdot f(t/n), \quad (5)$$

where $f(\cdot)$ is a monotonically increasing scheduling function that adjusts the transition pace based on training progress t/n . For θ where $\eta_{\text{init}} > \eta_{\text{final}}$, this formulation yields a reduction in θ from the easy to hard stage. Reversely, for ϕ and p where $\eta_{\text{init}} < \eta_{\text{final}}$, it results in an increase in ϕ/p to transition from easy to hard. We consider three variants of f :

- Linear: $f_1(x) = x$, corresponding to a uniform progression from easy to hard.
- Exponential (fast-to-slow): $f_2(x) = \frac{1 - \exp(-\lambda x)}{1 - \exp(-\lambda)}$, resulting in rapid initial changes that slow down gradually. $\lambda > 0$ controls the decay rate.
- Exponential (slow-to-fast): $f_3(x) = \frac{\exp(\lambda x) - 1}{\exp(\lambda) - 1}$, yielding slow initial changes but accelerating over time.

The three variants reflect different patterns of human learning. Some learners improve steadily, others learn

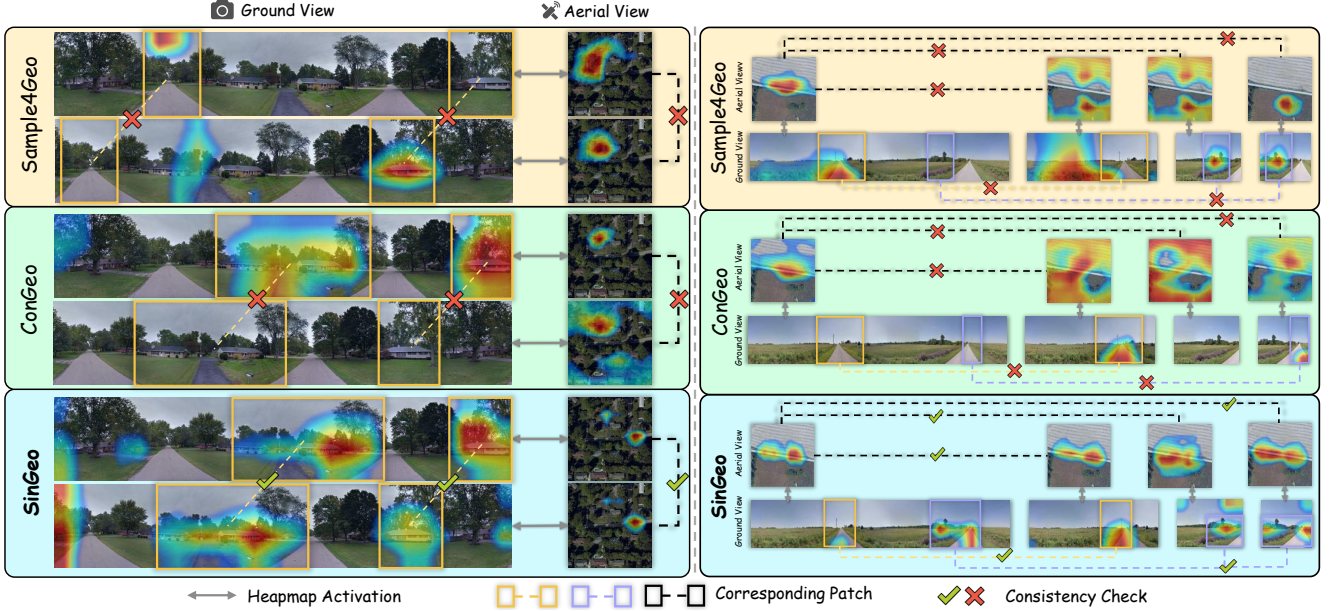


Figure 4. Visualization of consistency comparison among SinGeo, ConGeo and Sample4Geo on the CVUSA dataset. The left column depicts a sample under varying orientations, where SinGeo exhibits stronger consistency in both ground and satellite branches. The right column presents a sample under different FoVs, where the activation heatmaps of SinGeo remain stable across varying views.

quickly then refine gradually, or start slowly and accelerate later. A comparative analysis of these scheduling functions will be presented in our experiments.

4. Consistency: An Explainable and Quantitative Perspective

To understand the reasons behind SinGeo’s superior performance over existing methods in Fig. 1, we provide a visual explanation from the perspective of consistency through the lens of Grad-CAM [18]. The activation maps in Fig. 4 show that SinGeo maintains stable activated regions in both satellite and ground branches when the orientation or FoV changes. In contrast, previous methods exhibit dispersed or shifting activation. This observation suggests that SinGeo achieves more consistent cross-view matching, enabling it to generalize effectively beyond north-aligned panorama scenarios.

To explicitly formalize the notion of consistency, we obtain the activation heatmap \mathcal{H} of a query embedding e_{query} on its corresponding reference image I_{refer} using Grad-CAM [18], defined as:

$$\mathcal{H} = \text{GradCAM}(e_{\text{query}}, I_{\text{refer}}).$$

For a random orientation α and a given FoV θ , the transformed ground-view image is denoted as $I_g^*(\theta) = T_g(I_g | \alpha, \theta)$. Correspondingly, g and $g^*(\theta)$ are the embeddings of I_g and $I_g^*(\theta)$ encoded by \mathcal{E}_g , while s is the embedding of I_s encoded by the satellite encoder \mathcal{E}_s . We derive four heatmaps:

$$\begin{cases} \mathcal{H}_s = \text{GradCAM}(g, I_s) \\ \mathcal{H}_s^*(\theta) = \text{GradCAM}(g^*(\theta), I_s) \\ \mathcal{H}_g = \text{GradCAM}(s, I_g) \\ \mathcal{H}_g^*(\theta) = \text{GradCAM}(s, I_g^*(\theta)) \end{cases} \quad (6)$$

We apply the same transformation $T_g(\alpha, \theta)$ to \mathcal{H}_g , written as $T_g(\mathcal{H}_g | \alpha, \theta)$. A robust model should ensure that \mathcal{H}_s and $\mathcal{H}_s^*(\theta)$ remain consistent in the satellite branch, and that $T_g(\mathcal{H}_g | \alpha, \theta)$ and $\mathcal{H}_g^*(\theta)$ are also consistent in the ground branch. To quantify this consistency, we adopt the normalized Structural Similarity Index (SSIM) [27] and define two consistency metrics, orientation-consistency (OC) and FoV-consistency (FC), as follows:

$$\begin{cases} \text{OC}_{\text{sat}} = \text{SSIM}(\mathcal{H}_s, \mathcal{H}_s^*(360^\circ)) \\ \text{OC}_{\text{grd}} = \text{SSIM}(T_g(\mathcal{H}_g | \alpha, 360^\circ), \mathcal{H}_g^*(360^\circ)) \\ \text{FC}_{\text{sat}} = \frac{1}{3} \sum_{\theta_i \in \{180^\circ, 90^\circ, 70^\circ\}} \text{SSIM}(\mathcal{H}_s, \mathcal{H}_s^*(\theta_i)) \\ \text{FC}_{\text{grd}} = \frac{1}{3} \sum_{\theta_i \in \{180^\circ, 90^\circ, 70^\circ\}} \text{SSIM}(T_g(\mathcal{H}_g | \alpha, \theta_i), \mathcal{H}_g^*(\theta_i)) \end{cases} \quad (7)$$

5. Experiments

5.1. Experimental Setup

Datasets. We conduct experiments on four datasets. CVUSA [29] and CVACT [10] are two standard datasets for CVGL, featuring north-aligned, center-aligned panoramas and satellite images. CVUSA includes 35,532 image

Table 1. Comparison with single-model performance of state-of-the-art methods on CVUSA and CVACT Val datasets under unknown orientation and limited FoV settings. The results of methods with multiple FoV-specialized trained models are reported as reference with gray background. **Bold** indicates the best performance among single-model methods. Underline denotes the best performance across all methods. “-” denotes metrics not provided in the original paper.

Set	Methods	Avg. R@1	FoV 360°				FoV 180°				FoV 90°				FoV 70°			
			R@1	R@5	R@10	R@1%												
CVUSA	CVM-Net [6]	7.3	16.3	38.9	49.4	88.1	7.4	22.5	32.6	75.4	2.8	10.1	16.7	55.5	2.6	9.3	15.1	21.8
	CVFT [21]	10.0	23.4	44.4	55.2	86.6	8.1	24.3	34.5	75.2	4.8	14.8	23.2	61.2	3.8	12.4	19.3	55.6
	SEH [5]	40.9	85.4	93.5	95.8	-	53.7	72.3	79.0	-	16.6	32.2	40.3	-	7.8	18.8	25.6	-
	SAIG-D [34]	43.0	72.0	90.2	94.0	99.1	52.5	78.1	85.8	97.7	26.7	50.2	59.8	86.6	20.9	41.4	51.2	80.4
	GAL [16]	-	-	-	-	-	48.9	69.9	78.5	95.7	22.5	44.4	54.2	83.6	15.2	32.9	42.1	75.2
	DeHi [26]	-	82.4	93.5	96.3	99.4	60.4	81.8	88.2	98.0	31.5	55.1	65.6	90.8	-	-	-	-
	ArcGeo [23]	-	-	-	-	-	63.7	85.4	90.6	-	44.2	70.3	78.8	-	37.7	64.4	73.6	-
	Sample4Geo [3]	68.5	93.3	97.5	98.0	99.1	84.6	95.9	97.6	99.5	55.1	78.3	85.0	96.6	40.9	65.4	74.1	93.0
	SinGeo	79.1	96.8	99.0	99.2	99.5	91.8	97.6	98.4	99.5	70.1	86.6	91.0	97.5	58.0	78.1	83.9	95.2
	DSM [20]	37.9	78.1	89.5	92.9	98.5	48.5	68.5	75.6	93.0	16.2	31.4	39.9	71.1	8.8	19.9	27.3	61.2
	ConGeo [13]	73.4	96.6	98.9	99.2	99.7	<u>92.3</u>	<u>97.9</u>	<u>98.7</u>	<u>99.7</u>	55.5	75.4	81.5	93.9	49.1	70.8	78.0	93.1
CVACT	CVM-Net [6]	4.9	13.1	33.9	45.7	81.8	3.9	13.7	21.2	59.2	1.5	5.7	9.6	38.1	1.2	5.0	8.4	34.7
	CVFT [21]	10.9	26.8	46.9	55.1	81.0	8.1	24.3	34.5	75.2	4.8	14.8	23.2	61.2	3.8	12.4	19.3	55.6
	SEH [5]	36.5	77.4	88.6	90.9	-	47.7	67.9	74.3	-	13.9	28.4	36.2	-	6.9	16.5	22.3	-
	GAL [16]	-	-	-	-	-	49.9	68.5	77.2	93.0	26.1	49.2	59.3	85.6	14.2	33.0	43.2	77.2
	Sample4Geo [3]	47.0	82.4	90.6	92.3	95.4	58.9	79.8	85.3	95.0	27.9	52.0	62.3	87.0	18.8	40.4	51.0	81.3
	SinGeo	55.8	83.4	91.1	92.6	95.7	68.0	82.4	85.8	93.0	42.6	65.5	72.8	89.0	29.0	51.8	61.0	83.4
	DSM [20]	37.1	72.9	85.7	88.9	95.3	49.1	67.8	74.2	89.9	18.1	33.3	40.9	68.7	8.3	20.7	27.1	57.1
	ConGeo [13]	54.6	83.0	90.6	92.4	<u>96.3</u>	<u>70.3</u>	<u>85.2</u>	<u>88.6</u>	<u>95.1</u>	40.6	62.6	69.8	86.6	24.6	45.3	54.3	80.6

pairs for training and 8,884 for evaluation. CVACT has the same size for its training and validation sets, with an additional test set containing 92,802 pairs. VIGOR [32] is a challenging non-center-aligned dataset, containing 90,618 aerial-view and 105,214 ground-view images across four cities (New York, Seattle, San Francisco, Chicago). It uses two splits, namely same-area and cross-area: same-area uses all cities for training and validation, while cross-area conducts training on New York and Seattle and testing on San Francisco and Chicago for generalization evaluation. University-1652 [31] is a difficult CVGL dataset, containing ground-view images with unknown orientations and a limited FoV to evaluate models in real-world scenarios. Additionally, University-1652 offers a limited amount of data for training. For street-to-satellite matching, it only includes 2,579 street images and 951 satellite images, and for satellite-to-street matching, it comprises 701 satellite images and 2,921 street images.

Metrics. Following prior methods, we report retrieval performance using Top- k recall, denoted as $R@k$. For each query ground image, we retrieve the k nearest reference neighbors in the embedding space based on cosine similarity. A retrieval is correct if the ground-truth reference appears in the top k . Besides, we also report the new consistency metrics proposed in Sec. 4. In the main paper, we report SSIM-based consistency, while *supplementary material* includes consistency results based on cosine similarity and

pearson correlation coefficient [1].

Implementation Details. In the main experiments, we use ConvNeXt-B as our backbone. The weights ω_1 , ω_2 , ω_3 , and γ are set to 0.25, 0.25, 0.25, and 0.5 empirically. Label smoothing of 0.1 is used in the InfoNCE loss. To generate ground-view images with unknown orientation and limited FoV, $T_g^1(\alpha, \theta)$ or $T_g^2(\alpha, \theta)$ is used based on the backbone type. For satellite images, we use the discrete rotation $T_s^3(p)$ in main experiments. Additionally, for the curriculum scheduling function $f(x)$, we adopt the linear variant $f_1(x)$. Ablations of the three satellite rotation variants $T_s^1(\phi)$, $T_s^2(\phi)$, $T_s^3(p)$ and exponential scheduling function $f_2(x)$, $f_3(x)$ are provided in the *supplementary material*. The θ_{init} , θ_{final} are set to 360°, 70°, and the p_{init} , p_{final} are set to 100% and 25%. We choose Sample4Geo [3] as our baseline and train the model for 80 epochs with a batch size of 16. AdamW optimizer [12] is applied with an initial learning rate of 0.0001 and a cosine learning rate scheduler.

5.2. Comparison with State-of-the-art

CVUSA&CVACT: We evaluate SinGeo under scenarios involving both unknown orientations and limited FoVs on the CVUSA and CVACT validation sets in Tab. 1. Without FoV-specific training, our single model achieves SOTA performance across all scenarios on both CVUSA and CVACT. Moreover, SinGeo uses a single CNN backbone that surpasses multiple FoV-specialized trained models of DSM

Table 2. Comparison of state-of-the-art methods on CVUSA and CVACT datasets with north-aligned and center-aligned panorama-satellite pairs. The second-best performance is underlined.

Methods	CVUSA		CVACT Val		CVACT Test	
	R@1	R@1%	R@1	R@1%	R@1	R@1%
DSM [20]	92.0	99.7	82.5	97.3	-	-
DeHi [26]	94.3	<u>99.8</u>	85.0	98.6	-	-
TransGeo [33]	94.1	<u>99.8</u>	85.0	98.4	-	-
GeoDTR [30]	95.4	99.9	86.2	<u>98.8</u>	64.5	98.7
SAIG-D [34]	96.3	99.9	<u>89.1</u>	98.9	67.5	96.8
Sample4Geo [3]	98.7	99.9	<u>90.8</u>	<u>98.8</u>	71.5	98.7
SinGeo	<u>97.3</u>	99.9	87.1	96.9	<u>69.6</u>	97.1

Table 3. Comparison of methods on cross-area and same-area splits of VIGOR under unknown orientation and Limited FoV settings.

Methods	Cross-Area				Same-Area			
	FoV= 360°		FoV= 90°		FoV= 360°		FoV= 90°	
	R@1	R@1%	R@1	R@1%	R@1	R@1%	R@1	R@1%
VIGOR [32]	1.4	44.6	-	-	19.1	95.1	-	-
TransGeo [33]	5.5	66.9	-	-	47.7	99.3	-	-
Sample4Geo [3]	9.0	43.7	0.5	21.6	14.2	54.9	1.1	30.6
ConGeo [13]	16.2	72.9	3.9	54.3	61.9	98.4	8.5	68.7
SinGeo	24.7	85.7	4.9	63.7	62.9	98.4	24.0	91.5

and ConGeo. Although there is a slight drop compared to ConGeo at FoV= 180°, SinGeo exhibits significant improvements over ConGeo’s FoV-specific models in extreme cases of 90° and 70°. Notably, on the CVUSA dataset, SinGeo is the first model to surpass 70% and 50% on R@1 at FoV= 90° and FoV= 70°. We attribute this to the knowledge acquired during the early stages of curriculum learning, which substantially facilitates learning in extreme FoV conditions. Results on the CVACT test set are provided in the *supplementary material*.

Besides, we conduct experiments shown in Tab. 2 to demonstrate that SinGeo achieves superior robust CVGL without compromising its capability for traditional CVGL, where SinGeo still achieves competitive retrieval ability. The slight performance gap with Sample4Geo may be attributed to the latter’s specialized sampling strategy.

VIGOR. Previous research on robust CVGL has predominantly focused on evaluating models using center-aligned datasets, with limited exploration of non-center-aligned datasets such as VIGOR. Tab. 3 highlights the effectiveness of our approach on VIGOR. In the Same-Area subset, SinGeo outperforms existing methods with a remarkable 24.0% of R@1 and 91.5% of R@1% at 90°. This result once again demonstrates SinGeo’s robustness under extreme FoV conditions. In the Cross-Area subset, SinGeo shows comprehensive improvements compared with other methods, which reflects SinGeo’s ability to generalize across geographic regions under challenging conditions. Results under other

Table 4. Comparison of methods on St2S and S2St tasks of University-1652 dataset.

Methods	St2S		S2St	
	R@1	R@10	R@1	R@10
University-1652 [31]	0.6	5.51	0.9	6.0
LPN [25]	0.7	-	1.4	-
ConGeo [13]	5.9	-	6.8	-
SinGeo	5.9	23.73	7.1	22.8

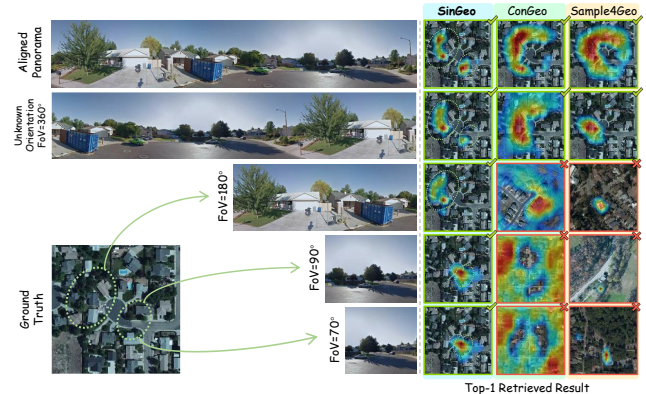


Figure 5. Qualitative evaluation on a sample of CVUSA dataset. Left: A query image under varied orientations and FoVs, together with its ground-truth satellite image. Right: Top-1 retrieved images and activated heatmap regions of different methods. Green circles denote the regions on the satellite image that correspond to the limited-FoV ground images.

FoVs are provided in the *supplementary material*.

University-1652. Without panorama provided, we use two distinct ground-view images captured at the same location, following [13], denoted as (I_g^1, I_g^2) , to replace (I_g, I_g^*) in our learning objective, and only activate the satellite image rotation transformation during training. As shown in Tab. 4, due to high task difficulty and limited data, LPN and the University-1652 baseline perform worse than SinGeo and ConGeo. Through a richer contrastive learning pipeline, SinGeo enables more effective feature extraction and achieves better overall results under data scarcity and constraints.

5.3. Consistency Evaluation

We conduct consistency evaluation starting from a single sample. Fig. 5 shows that SinGeo achieves the best performance with consistent heatmap activations. For panoramas with unknown orientations, although other methods retrieve correctly, their focused regions shift or diverge, which is undesirable since the two panoramas contain the same information. When the FoV narrows, only SinGeo retrieves correct results because its focused regions remain well aligned with the corresponding ground areas. Furthermore, the regions that SinGeo focuses on for limited-FoV images are also focused for panoramas, showing that SinGeo can extend its

Table 5. Quantitative evaluation of orientation-consistency(OC) and FoV-consistency(FC) on CVUSA dataset.

Method	OC _{grd}	OC _{sat}	FC _{grd}	FC _{sat}
Sample4Geo [3]	0.65	0.67	0.50	0.66
ConGeo [13]	0.38	0.71	0.35	0.68
SinGeo	0.81	0.92	0.66	0.76

Table 6. Cross-architecture generalization on the CVUSA dataset under unknown orientation and limited FoV settings.

Methods	FoV= 360°		FoV= 180°		FoV= 90°	
	R@1	R@1%	R@1	R@1%	R@1	R@1%
GeoDTR [30]	7.1	30.6	3.1	19.6	0.5	8.9
+ConGeo [13]	44.5	96.2	32.9	92.9	13.3	71.4
+SinGeo	54.8	98.2	37.1	95.9	17.8	82.8
Sample4Geo[CNN] [3]	93.3	99.1	84.6	99.5	55.1	96.6
+ConGeo [13]	85.2	98.9	92.3	99.7	55.9	90.9
+SinGeo	96.8	99.5	91.8	99.5	70.1	97.5
Sample4Geo[ViT] [3]	16.7	45.6	11.3	41.7	3.7	29.6
+ConGeo [13]	19.7	68.1	65.8	94.9	34.5	80.2
+SinGeo	76.0	96.5	72.4	97.2	44.8	89.6

capability from north-aligned panoramas to other scenarios.

Besides, we conduct the consistency quantitative evaluation on CVUSA validation dataset of 8884 image pairs in Tab. 5. SinGeo maintains the highest consistency in both satellite and ground branches under different variations.

We argue that the high consistency of SinGeo is highly correlated with its strong recall performance under unknown orientations and limited FoVs, as SinGeo can extend its excellent performance in north-aligned scenarios to other situations. This finding is intended to inspire future research enabling models to maintain higher consistency through novel designs, thereby achieving better robustness.

5.4. Cross-architecture Generalization

An important characteristic of SinGeo is its model-agnostic nature. We transfer the training strategy of SinGeo into different architectures to boost their robustness. In particular, we selected two backbone variants of Sample4Geo—ViT [4] and ConvNeXt [3], and a CNN-Attention hybrid model, GeoDTR [30]. Besides, we compared the boosting efficacy with another plug-and-play method, ConGeo [13]. Since ConGeo only supports FoV-fixed training, following its original paper, we trained ConGeo at FoV=180°, enabling it to achieve the highest average R@1.

In Tab. 6, SinGeo exhibits better robustness across architectures than ConGeo and baselines, with significant enhancements on ViT variant of Sample4Geo, boosting R@1 from 16.7% to 76.0% at 360°FoV. Also notably, SinGeo elevates GeoDTR’s R@1 by more than 47% under 360° FoV. These results validate the advantage of the curriculum-

Table 7. Ablations under different DDL and CL configurations on the CVUSA dataset.

DDL	CL	FoV= 360°		FoV= 180°		FoV= 90°	
		R@1	R@1%	R@1	R@1%	R@1	R@1%
I_g^*	I_s^*						
×	×	93.3	99.1	84.6	99.5	55.1	96.6
✓	×	85.2	98.9	92.3	99.7	55.9	90.9
✓	✓	91.5	99.3	80.6	98.3	47.8	87.7
✓	×	96.2	99.5	92.1	99.5	66.9	96.4
✓	✓	96.8	99.5	91.8	99.5	70.1	97.5

inspired FoV training paradigm over fixed-FoV paradigms.

5.5. Ablation Study

To validate the efficacy of the proposed dual discriminative learning (DDL) architecture and curriculum learning (CL) strategy, we perform an ablation study on the CVUSA dataset to verify their contributions to robustness. As shown in Tab. 7, incorporating I_g^* alone enhances performance at 180°FoV with 92.3% of R@1, but degrades at 360° and 90° compared to the baseline. Adding both I_g^* and I_s^* improves 360°R@1% but harms performance under limited FoVs. CL boosts robustness, particularly at 90°, and yields the best overall results combined with full DDL. The ablation confirms the synergy between DDL and CL for consistent cross-FoV performance. Ablations among different rotation transformations, scheduling functions and the weights $\omega_1, \omega_2, \omega_3, \gamma$ are provided in the *supplementary material*.

6. Conclusion and Limitation

In this work, we presented SinGeo, a new paradigm for robust CVGL. SinGeo leverages a dual discriminative learning architecture, treating both ground and satellite branches equally and strengthening intra-view discriminability. SinGeo also introduces a curriculum learning strategy guiding the model in a natural manner. Extensive experiments on four benchmarks indicate that SinGeo uses only a single backbone and surpasses existing methods by a large margin under varying orientations and FoVs. These results provide a clear answer to the question raised in our introduction: a single backbone can indeed achieve consistent and high performance across diverse conditions, without additional modules or explicit transformations. Moreover, SinGeo can be transferred to other CVGL methods to further boost their robustness, outperforming FoV-specialized paradigm enhancement. Beyond performance, our consistency evaluation provides a perspective for understanding robustness in CVGL, showing that stable model responses across scenarios are highly correlated with robust retrieval.

Admittedly, SinGeo requires the prior knowledge of panoramas during training. How to achieve excellent performance using datasets without aligned panoramas, such as University-1652 [31], remains a challenge in CVGL.

References

- [1] Jacob Benesty, Jingdong Chen, Yiteng Huang, and Israel Cohen. Pearson correlation coefficient. In *Noise reduction in speech processing*, pages 1–4. Springer, 2009. 6, 2
- [2] Yoshua Bengio, Jérôme Louradour, Ronan Collobert, and Jason Weston. Curriculum learning. In *Proceedings of the 26th annual international conference on machine learning*, pages 41–48, 2009. 2
- [3] Fabian Deuser, Konrad Habel, and Norbert Oswald. Sample4geo: Hard negative sampling for cross-view geo-localisation. In *Proceedings of the IEEE/CVF International Conference on Computer Vision*, pages 16847–16856, 2023. 1, 2, 4, 6, 7, 8, 3
- [4] Alexey Dosovitskiy, Lucas Beyer, Alexander Kolesnikov, Dirk Weissenborn, Xiaohua Zhai, Thomas Unterthiner, Mostafa Dehghani, Matthias Minderer, Georg Heigold, Sylvain Gelly, Jakob Uszkoreit, and Neil Houlsby. An image is worth 16x16 words: Transformers for image recognition at scale. In *International Conference on Learning Representations*, 2021. 2, 8
- [5] Yulan Guo, Michael Choi, Kunhong Li, Farid Boussaid, and Mohammed Bennamoun. Soft exemplar highlighting for cross-view image-based geo-localization. *IEEE transactions on image processing*, 31:2094–2105, 2022. 1, 2, 6
- [6] Sixing Hu, Mengdan Feng, Rang MH Nguyen, and Gim Hee Lee. Cvm-net: Cross-view matching network for image-based ground-to-aerial geo-localization. In *Proceedings of the IEEE Conference on Computer Vision and Pattern Recognition*, pages 7258–7267, 2018. 1, 2, 6
- [7] Ang Li, Huiyi Hu, Piotr Mirowski, and Mehrdad Farajtabar. Cross-view policy learning for street navigation. In *Proceedings of the IEEE/CVF international conference on computer vision*, pages 8100–8109, 2019. 1
- [8] Guopeng Li, Ming Qian, and Gui-Song Xia. Unleashing unlabeled data: A paradigm for cross-view geo-localization. In *Proceedings of the IEEE/CVF Conference on Computer Vision and Pattern Recognition*, pages 16719–16729, 2024. 2
- [9] Tsung-Yi Lin, Serge Belongie, and James Hays. Cross-view image geolocalization. In *Proceedings of the IEEE Conference on Computer Vision and Pattern Recognition*, pages 891–898, 2013. 1
- [10] Liu Liu and Hongdong Li. Lending orientation to neural networks for cross-view geo-localization. In *Proceedings of the IEEE/CVF Conference on Computer Vision and Pattern Recognition*, pages 5624–5633, 2019. 1, 2, 5
- [11] Zhuang Liu, Hanzi Mao, Chao-Yuan Wu, Christoph Feichtenhofer, Trevor Darrell, and Saining Xie. A convnet for the 2020s. In *Proceedings of the IEEE/CVF Conference on Computer Vision and Pattern Recognition*, pages 11976–11986, 2022. 2
- [12] Ilya Loshchilov and Frank Hutter. Decoupled weight decay regularization. In *International Conference on Learning Representations*, 2017. 6
- [13] Li Mi, Chang Xu, Javiera Castillo-Navarro, Syrielle Montariol, Wen Yang, Antoine Bosselut, and Devis Tuia. Congeo: Robust cross-view geo-localization across ground view variations. In *European Conference on Computer Vision*, 2024. 1, 2, 3, 6, 7, 8
- [14] Aaron van den Oord, Yazhe Li, and Oriol Vinyals. Representation learning with contrastive predictive coding. *arXiv preprint arXiv:1807.03748*, 2018. 2, 3
- [15] Joshua Robinson, Li Sun, Ke Yu, Kayhan Batmanghelich, Stefanie Jegelka, and Suvrit Sra. Can contrastive learning avoid shortcut solutions? *Advances in neural information processing systems*, 34:4974–4986, 2021. 3
- [16] Royston Rodrigues and Masahiro Tani. Global assists local: Effective aerial representations for field of view constrained image geo-localization. In *Proceedings of the IEEE/CVF Winter Conference on Applications of Computer Vision*, pages 3871–3879, 2022. 1, 2, 3, 6
- [17] Florian Schroff, Dmitry Kalenichenko, and James Philbin. Facenet: A unified embedding for face recognition and clustering. In *2015 IEEE Conference on Computer Vision and Pattern Recognition (CVPR)*, pages 815–823, 2015. 3
- [18] Ramprasaath R Selvaraju, Michael Cogswell, Abhishek Das, Ramakrishna Vedantam, Devi Parikh, and Dhruv Batra. Grad-cam: Visual explanations from deep networks via gradient-based localization. In *Proceedings of the IEEE international conference on computer vision*, pages 618–626, 2017. 5
- [19] Yujiao Shi, Liu Liu, Xin Yu, and Hongdong Li. Spatial-aware feature aggregation for cross-view image based geo-localization. *Advances in Neural Information Processing Systems*, 32, 2019. 2
- [20] Yujiao Shi, Xin Yu, Dylan Campbell, and Hongdong Li. Where am i looking at? joint location and orientation estimation by cross-view matching. In *Proceedings of the IEEE/CVF Conference on Computer Vision and Pattern Recognition*, pages 4064–4072, 2020. 1, 2, 6, 7
- [21] Yujiao Shi, Xin Yu, Liu Liu, Tong Zhang, and Hongdong Li. Optimal feature transport for cross-view image geo-localization. In *Proceedings of the AAAI Conference on Artificial Intelligence*, pages 11990–11997, 2020. 2, 6
- [22] Tavis Shore, Simon Hadfield, and Oscar Mendez. Bev-cv: Birds-eye-view transform for cross-view geo-

- localisation. In *2024 IEEE/RSJ International Conference on Intelligent Robots and Systems (IROS)*, pages 11048–11055. IEEE, 2024. [1](#), [2](#)
- [23] Maxim Shugaev, Ilya Semenov, Kyle Ashley, Michael Klaczynski, Naresh Cuntoor, Mun Wai Lee, and Nathan Jacobs. Arcgeo: Localizing limited field-of-view images using cross-view matching. In *Proceedings of the IEEE/CVF Winter Conference on Applications of Computer Vision*, pages 209–218, 2024. [1](#), [2](#), [3](#), [6](#)
- [24] Nam N Vo and James Hays. Localizing and orienting street views using overhead imagery. In *European conference on computer vision*, pages 494–509. Springer, 2016. [2](#), [3](#)
- [25] Tingyu Wang, Zhedong Zheng, Chenggang Yan, Jiyong Zhang, Yaoqi Sun, Bolun Zheng, and Yi Yang. Each part matters: Local patterns facilitate cross-view geo-localization. *IEEE Transactions on Circuits and Systems for Video Technology*, 32(2):867–879, 2021. [7](#)
- [26] Teng Wang, Jiawen Li, and Changyin Sun. Dehi: A decoupled hierarchical architecture for unaligned ground-to-aerial geo-localization. *IEEE Transactions on Circuits and Systems for Video Technology*, 34(3):1927–1940, 2023. [1](#), [2](#), [6](#), [7](#)
- [27] Zhou Wang. Image quality assessment: from error visibility to structural similarity. *IEEE Transactions on Image Processing*, 13(4):600–612, 2004. [5](#), [2](#)
- [28] Junyan Ye, Zhutao Lv, Weijia Li, Jinhua Yu, Haote Yang, Huaping Zhong, and Conghui He. Cross-view image geo-localization with panorama-bev co-retrieval network. In *European Conference on Computer Vision*, pages 74–90. Springer, 2024. [2](#)
- [29] Menghua Zhai, Zachary Bessinger, Scott Workman, and Nathan Jacobs. Predicting ground-level scene layout from aerial imagery. In *Proceedings of the IEEE Conference on Computer Vision and Pattern Recognition*, pages 867–875, 2017. [1](#), [2](#), [5](#)
- [30] Xiaohan Zhang, Xingyu Li, Waqas Sultani, Yi Zhou, and Safwan Wshah. Cross-view geo-localization via learning disentangled geometric layout correspondence. In *Proceedings of the AAAI conference on artificial intelligence*, pages 3480–3488, 2023. [1](#), [2](#), [7](#), [8](#)
- [31] Zhedong Zheng, Yunchao Wei, and Yi Yang. University-1652: A multi-view multi-source benchmark for drone-based geo-localization. In *Proceedings of the 28th ACM international conference on Multimedia*, pages 1395–1403, 2020. [6](#), [7](#), [8](#)
- [32] Sijie Zhu, Taojiannan Yang, and Chen Chen. Vigor: Cross-view image geo-localization beyond one-to-one retrieval. In *Proceedings of the IEEE/CVF Conference on Computer Vision and Pattern Recognition*, pages 3640–3649, 2021. [6](#), [7](#), [2](#)
- [33] Sijie Zhu, Mubarak Shah, and Chen Chen. Transgeo: Transformer is all you need for cross-view image geo-localization. In *Proceedings of the IEEE/CVF Conference on Computer Vision and Pattern Recognition*, pages 1162–1171, 2022. [1](#), [2](#), [3](#), [7](#)
- [34] Yingying Zhu, Hongji Yang, Yuxin Lu, and Qiang Huang. Simple, effective and general: A new backbone for cross-view image geo-localization. *arXiv preprint arXiv:2302.01572*, 2023. [1](#), [6](#), [7](#)

SinGeo: Unlock Single Model’s Potential for Robust Cross-View Geo-Localization

Supplementary Material

In this supplementary material, we provide the following information for the completeness of our paper.

- Ablations of different rotation transformations (Section A).
- Ablations of different scheduling functions (Section B).
- Ablations of different loss weights (Section C).
- Performance on CVACT test set (Section D).
- Supplementary results on VIGOR (Section E).
- Consistency metrics based on cosine similarity and pearson correlation coefficient (Section F).
- Additional qualitative visualization results (Section G).
- Implementation details (Section H).

A. Ablations of Different Rotation Transformations

Table 8. Performance comparison of different rotation transformations for I_s on the CVUSA dataset.

Transformations	FoV= 360°		FoV= 180°		FoV= 90°	
	R@1	R@1%	R@1	R@1%	R@1	R@1%
$T_s^1(\phi)$	89.2	97.3	77.5	94.2	63.7	96.4
$T_s^2(\phi)$	88.9	97.5	81.1	97.4	60.7	95.8
$T_s^3(p)$	96.8	99.5	91.8	99.5	70.1	97.5

We compare the performance of proposed $T_s^1(\phi)$, $T_s^2(\phi)$, and $T_s^3(p)$ on CVUSA dataset. In Tab. 8, the discrete rotation transformation $T_s^3(p)$ consistently outperforms the continuous variants $T_s^1(\phi)$ and $T_s^2(\phi)$ across all FoVs on the CVUSA dataset. We assume that discrete rotation transformations outperform continuous ones because the former can avoid introducing additional padding boundaries and will not cause information loss. Discrete 90° multiples enable exact pixel permutations, preserving discriminative features.

B. Ablations of Different Scheduling Functions

Table 9. Performance comparison of different scheduling functions on the CVUSA dataset.

Scheduling Function	Avg. R@1	FoV= 360°		FoV= 180°		FoV= 90°	
		R@1	R@1%	R@1	R@1%	R@1	R@1%
$f_1(x)$	86.2	96.8	99.5	91.8	99.5	70.1	97.5
$f_2(x)(\lambda = 3)$	79.9	94.6	99.6	83.7	99.2	61.5	96.0
$f_3(x)(\lambda = 3)$	82.8	97.1	99.8	90.9	99.3	60.4	92.3
$f_2(x)(\lambda = 5)$	82.0	95.8	99.5	83.1	98.3	67.0	96.2
$f_3(x)(\lambda = 5)$	82.3	96.6	99.8	89.8	99.6	60.5	94.5
<i>Random</i>	76.7	90.3	98.7	83.6	98.8	56.2	93.5

We also considered different scheduling functions. As observed in Tab. 9, a simple linear scheduling function $f_1(x)$ achieves superior overall performance with 86.2 of average R@1 compared to alternative exponential variants $f_2(x)$, $f_3(x)$ and random scheduling. Notably, all scheduling functions that progress from easy to hard outperform random scheduling, as the latter lacks a progressive adaptation mechanism. We hypothesize that the linear schedule maintains a constant gradient in training difficulty between epochs, thereby mitigating abrupt shifts that could lead to model instability, such as insufficient adaptation to escalating challenges. This result validates that a straightforward progressive training paradigm is highly beneficial for model to learn robustness.

C. Ablations of Different Loss Weights

Table 10. Performance comparison of different loss weight configurations on the CVUSA dataset.

γ	$\omega_1\omega_2\omega_3$	Avg. R@1	FoV= 360°		FoV= 180°		FoV= 90°	
			R@1	R@1%	R@1	R@1%	R@1	R@1%
0.5	0.25	86.1	96.8	99.5	91.5	99.4	70.1	97.5
0.5	0.5	84.7	96.2	99.6	90.0	99.4	68.0	97.7
0.25	0.5	85.6	96.4	99.7	90.7	99.6	69.6	97.6
0.25	0.25	85.8	96.7	99.7	90.2	99.2	70.6	97.6

In Tab. 10, we look into the effect of loss weights γ and $\omega_1, \omega_2, \omega_3$ on performance. Results show that different weight configurations cause minor performance fluctuations across FoV settings. The default setup $\gamma = 0.5, \omega = 0.25$ achieves the best average R@1 of 86.1 and outperforms other configurations at FoV= 360° and FoV= 180°.

D. Performance on CVACT Test Set

In the main paper, we reported the results on CVACT validation set. In this section, we also evaluate SinGeo on the CVACT test set under unknown orientation and limited FoV settings as shown in Tab. 11, comparing it with Sample4Geo [3] and two FoV-specialized ConGeo variants [13]. ConGeo[360] and ConGeo[180] are trained specifically at 360° and 180° FoV respectively, showing strong performance at their trained angles but significant degradation at unseen narrow FoVs.

In contrast, SinGeo uses a single model without FoV-specific training and achieves the best average R@1 of 35.8 across all FoVs. It outperforms both ConGeo variants at every FoV except 180° where ConGeo[180] holds a marginal

Table 11. Comparison with single-model performance of selected methods on CVACT Test dataset under unknown orientation and limited FoV settings.

Methods	Avg.	FoV 360°				FoV 180°				FoV 90°				FoV 70°			
	R@1	R@1	R@5	R@10	R@1%												
Sample4Geo[3]	2.4	8.0	12.5	14.0	31.0	1.0	2.7	3.8	25.1	0.4	1.3	2.2	24.1	0.2	0.7	1.1	16.9
ConGeo[360][13]	25.0	64.3	81.5	84.7	95.6	28.6	47.8	54.9	88.4	5.2	13.0	17.9	67.8	1.8	5.6	8.4	53.3
ConGeo[180][13]	25.4	37.4	55.3	61.1	89.6	45.6	67.1	73.0	94.3	13.7	28.3	35.6	81.7	5.0	13.1	18.0	68.6
SinGeo	35.8	66.7	84.2	86.8	96.0	46.0	66.8	72.6	93.2	19.6	38.8	47.1	89.3	11.0	25.5	33.3	84.2

Table 12. Comparison of methods on cross-area and same-area splits of VIGOR under unknown orientation and limited FoV settings. “-” denotes metrics not provided in the original paper.

Set	Methods	FoV 360°				FoV 180°				FoV 90°				FoV 70°				
		R@1	R@5	R@10	R@1%													
Cross-Area	VIGOR [32]	1.4	-	-	44.6	-	-	-	-	-	-	-	-	-	-	-	-	-
	TransGeo [33]	5.5	-	-	66.9	-	-	-	-	-	-	-	-	-	-	-	-	-
	Sample4Geo [3]	9.0	-	-	43.7	-	-	-	-	0.5	-	-	21.6	-	-	-	-	-
	ConGeo [13]	16.2	-	-	72.9	-	-	-	-	3.9	-	-	54.3	-	-	-	-	-
	SinGeo	24.7	43.5	51.4	85.7	11.0	24.0	30.7	72.6	4.9	12.9	18.2	63.7	3.3	9.2	13.2	56.0	
Same-Area	VIGOR [32]	19.1	-	-	95.1	-	-	-	-	-	-	-	-	-	-	-	-	-
	TransGeo [33]	47.7	-	-	99.3	-	-	-	-	-	-	-	-	-	-	-	-	-
	Sample4Geo [3]	14.2	-	-	54.9	-	-	-	-	1.1	-	-	30.6	-	-	-	-	-
	ConGeo [13]	61.9	-	-	98.4	-	-	-	-	8.5	-	-	68.7	-	-	-	-	-
	SinGeo	62.9	88.5	91.5	98.0	43.0	69.0	75.2	94.0	24.0	46.3	54.6	91.5	16.1	34.2	42.3	85.5	

edge in R@5 and R@10. Notably, SinGeo maintains best performance even at extreme narrow FoVs.

E. Supplementary Results on VIGOR

In the main paper, we reported results of VIGOR dataset at 360° and 90° FoV. We further supplement results at 180° and 70° FoV as shown in Tab. 12. SinGeo achieves excellent performance on VIGOR, a non-center-aligned dataset, outperforming other compared methods across both Cross-Area and Same-Area splits.

F. The Consistency Metrics Based on Cosine Similarity and PCC

Table 13. Quantitative evaluation of orientation-consistency(OC) and FoV-consistency(FC) on CVUSA dataset based on cosine similarity and pearson correlation coefficient).

Metric	Method	OC _{grd}	OC _{sat}	FC _{grd}	FC _{sat}
Cosine Similarity	Sample4Geo [3]	0.37	0.40	0.25	0.32
	ConGeo [13]	0.15	0.61	0.22	0.46
	SinGeo	0.77	0.91	0.54	0.63
PCC	Sample4Geo [3]	0.13	0.18	0.04	0.11
	ConGeo [13]	0.10	0.46	0.17	0.21
	SinGeo	0.65	0.89	0.31	0.54

In the main paper, we adopt the Structural Similarity

Index (SSIM) [27], a classic 2D similarity measurement method, to calculate the consistency between activation heatmaps. To further validate our conclusions, we flatten the 2D heatmaps into 1D tensors and utilize cosine similarity and Pearson Correlation Coefficient (PCC) [1] to compute the consistency metrics between these tensors. As shown in Tab. 13, SinGeo still achieves the highest scores across all orientation-consistency (OC) and FoV-consistency (FC) metrics when using cosine similarity and PCC. These results confirm that SinGeo preserves stable activation under orientation shifts and FoV variations.

G. Additional Qualitative Visualization Results

We further provide supplementary qualitative visualizations in Fig. 6, Fig. 7 and Fig. 8. When the aligned panorama is applied with a random translation (the second row), SinGeo maintains consistent responses on satellite images. As the FoV further narrows (last three rows), the model consistently responds to key semantic regions of satellite images that correspond to the ground images (the yellow dashed circles). Compared with SinGeo, the results of ConGeo and Sample4Geo are less satisfactory. Even when retrieval is correct, their response regions show certain shifts or errors. As shown in the first and second rows of Fig. 6, after panorama translation, ConGeo’s responses on satellite images become completely different despite identical information in panoramas. As shown in the third row of Fig. 6, when FoV=180°,

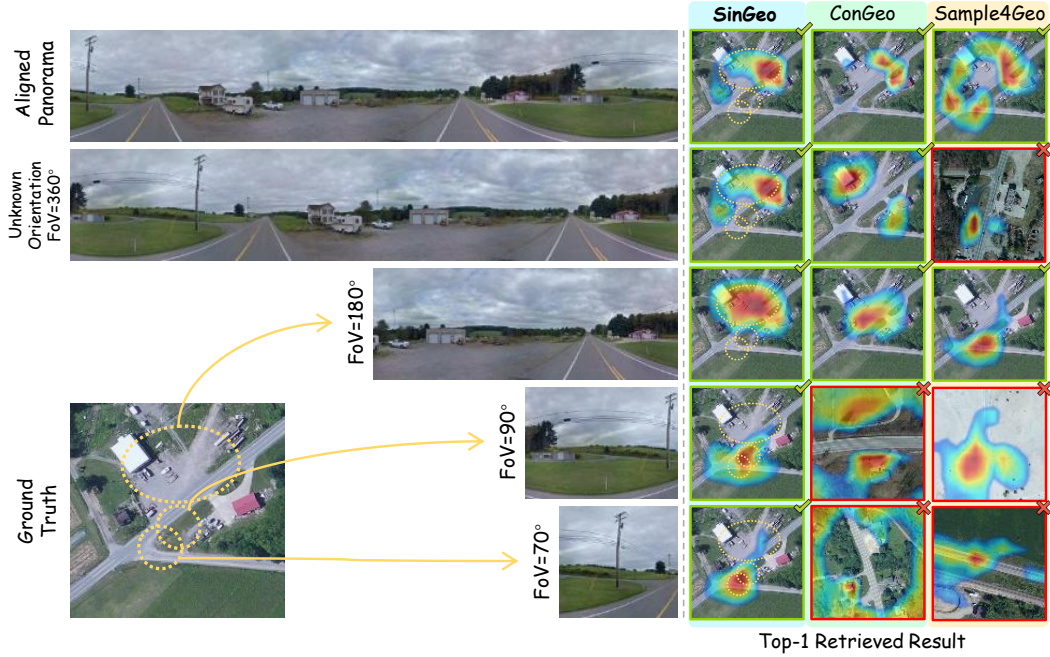


Figure 6. Qualitative visualization result on CVUSA. Yellow circles denote the regions on the satellite image that correspond to the limited-FoV ground images.

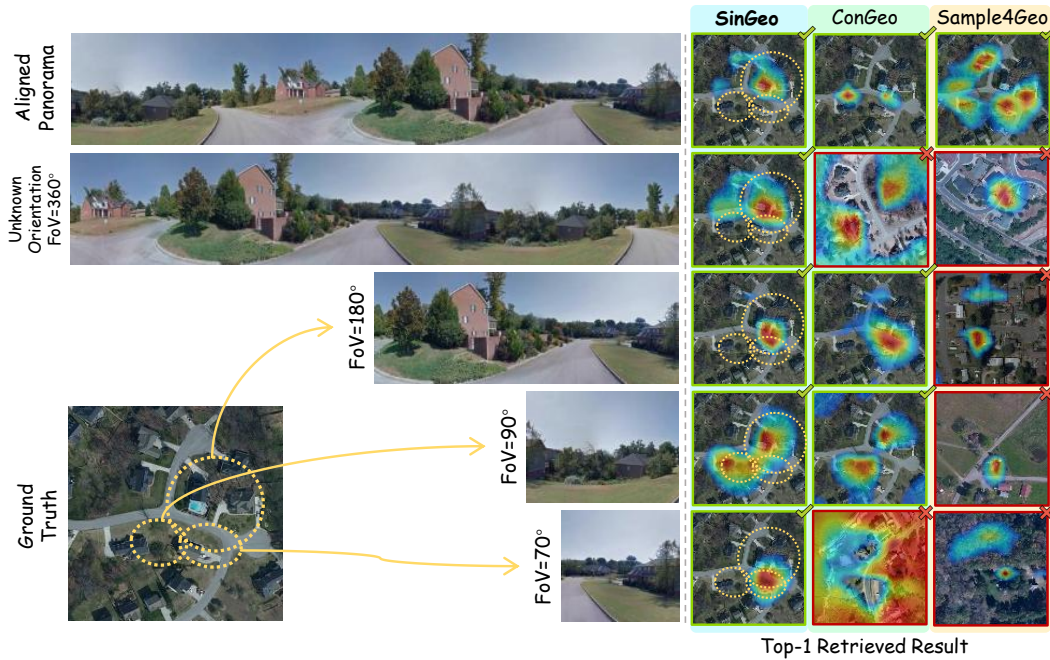


Figure 7. Qualitative visualization result on CVUSA. Yellow circles denote the regions on the satellite image that correspond to the limited-FoV ground images.

Sample4Geo’s response region does not match the corresponding area of the ground query image even with correct retrieval.

H. Implementation Details

We follow the data preprocessing method of our baseline Sample4Geo [3]. Our code of this paper uses Python 3.8.20, PyTorch 2.1.1, timm 0.9.0, and scikit-learn 1.3.2. All train-

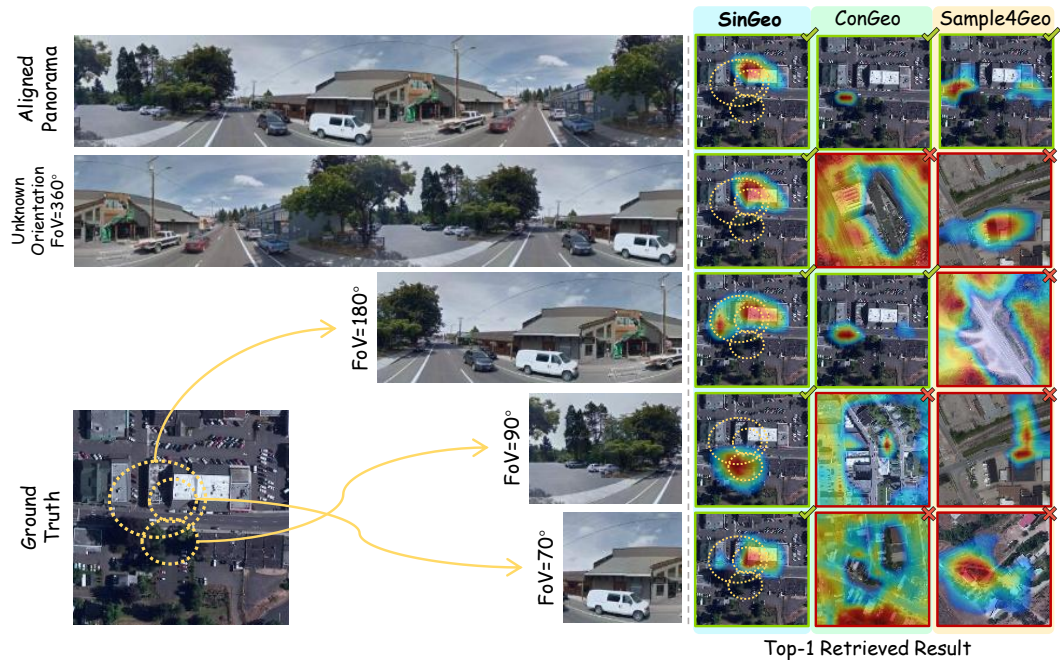


Figure 8. Qualitative visualization result on CVUSA. Yellow circles denote the regions on the satellite image that correspond to the limited-FoV ground images.

ing and testing are conducted on a single NVIDIA A100 GPU.